Nonorthogonal Replication Scheme for ALOHA Uplink in LPWAN

Jean Michel de Souza Sant'Ana, *Student Member, IEEE*, Samuel Montejo-Sánchez, *Senior Member, IEEE*, Richard Demo Souza, *Senior Member, IEEE*, and Hirley Alves, *Member, IEEE*

***Abstract*—In this work, we address a novel replication scheme for Internet-of-Things low-power wide area networks, considering the ability of a gateway to recover, through successive interference cancellation (SIC), superposed signals in the power domain. We show that the introduced mathematical framework matches the Monte Carlo simulations. The proposed scheme outperforms typical transmission schemes, at least from 1 to 2 orders of magnitude, in terms of outage probability. We also show that the scheme fits well with previous replication schemes, outperforming their versions without nonorthogonal replications. Moreover, we show that the proposed scheme can be robust to cases with high SIC imperfection, presenting slight performance losses even in very harsh scenarios, as long as the constraints are met. Finally, we conclude that the proposed scheme can be more energy efficient than previous replication schemes and achieve better reliability in traffic-loaded networks.**

***Index Terms*—ALOHA, low-power wide area networks (LPWAN), message replication, nonorthogonality, reliability, successive interference cancellation.**

I. Introduction

THE importance of machine-type communications (MTC) keeps exponentially growing, driven by the interest in the Internet-of-Things (IoT) [1]. One important example is the development of the 5 G use cases, where two-thirds of them were built specifically to cover MTC cases. Ultrareliable low-latency communications focus on critical MTC applications, where the goal is to deliver information within very restrictive latency and reliability requirements. Moreover, massive MTC (mMTC) addresses cases where it should serve an enormous amount of devices with not so strict delay and reliability requirements [2].

Even though the 5 G standardization efforts, the development of mMTC does not cover all the industry needs [3]. This creates space for the rising of other technologies, leading to integrated heterogeneous scenarios [4]. Thus, low-power wide area networks (LPWAN) stand as an alternative to the communication layer for IoT applications [5], where they present high energy efficiency, long range, low cost, and great uplink performance [6]. So far, the two most prominent LPWAN technologies are Sigfox[1] and LoRa wide area network (LoRaWAN). Each of them has its own specificity, such as business plan, setup, and communication parameters. However, both networks present similar behaviors, as seamless connection to base stations, large link budgets, very low transmission rate, and energy consumption [7]. Sigfox and LoRaWAN present none to very limited signalling to save energy and hardware complexity. However, this brings limitations in terms of scalability, as an increased number of devices cause a higher amount of collisions due to the lack of transmission coordination.

This article focuses on investigating the use of nonorthogonal replications on LPWAN technologies. We aim to boost the reliability of those technologies without increasing the amount of traffic and energy consumption as traditional replication schemes, and then increasing their energy efficiency. We analyze and compare the success probability, energy consumption, and spectral efficiency of the proposed nonorthogonal replication scheme against regular transmission and other replication schemes. The results are based on a system model first introduced in [8] and [9]. Finally, Monte Carlo simulations validate our theoretical results.

A. Related Work

There are several recent works presenting techniques to increase the performance of LPWAN technologies. Some works focused on coding and replication techniques [10], [11], [12], [13], [14], while there are works handling specific parameter selection [15], [16], [17], and use cases in industrial scenarios [18], [19], [20], [21], although some of their results can be extended to

Manuscript received 28 October 2022; revised 14 February 2023 and 6 March 2023; accepted 7 May 2023. Date of publication 26 May 2023; date of current version 19 January 2024. This work was supported in part by the Academy of Finland, 6G Flagship program under Grant 346208, in part by the Brazil by CNPq under Grant 402378/2021-0, Grant 305021/2021-4, and Grant 401730/2022-0, and in part by the Chile by ANID FONDECYT Iniciación under Grant 11200659. Paper no. TII-22-4472. *(Corresponding author: Jean Michel de Souza Sant'Ana.)*

Jean Michel de Souza Sant'Ana and Hirley Alves are with the Centre for Wireless Communications, University of Oulu, 90570 Oulu, Finland (e-mail: jean.desouzasantana@oulu.fi; hirley.alves@oulu.fi).

Samuel Montejo-Sánchez is with the Programa Institucional de Fomento a la Investigación, Desarrollo e Innovación, Universidad Tecnológica Metropolitana, Santiago 8940577, Chile (e-mail: smontejo@utem.cl).

Richard Demo Souza is with the Department of Electrical and Electronics Engineering, Federal University of Santa Catarina, Florianóplis 88040-900, Brazil (e-mail: richard.demo@ufsc.br).

Color versions of one or more figures in this article are available at https://doi.org/10.1109/TII.2023.3280315.

Digital Object Identifier 10.1109/TII.2023.3280315

[1] In 2022, Sigfox was acquired by Unabiz.

any generic use case. Finally, the research activity on decoding multiple colliding signals for LPWAN [22], [23], [24], [25], [26] has increased.

Georgiou and Raza [8] presented a stochastic approach for LoRaWAN, and highlighted the limitations of the network with an increased number of users, which is also shown in [9], considering imperfect orthogonality. Several works addressed the scalability of such networks and proposed techniques to increase the reliability. For example, the authors in [10] and [11] investigated the impact of message replication in SigFox and LoRaWAN-like networks, respectively. Both of them state that there is an optimal number of replications, where, after this point, the collisions grow faster than the reliability gain. Considering application level codification, [12] and [13] proposed and evaluated two packet coding schemes for LPWAN. Both works conclude that coding the messages across packets results in better reliability. Sant'Ana et al. [14] generalized the coding scheme from [13], adding two new input parameters. Such a new set of parameters allows the network administrator to fine-tune the coding scheme for each scenario.

A few works have considered a fixed distance-based scheme [8], [9], [11]. However, this proved inefficient, and then works considering the amount of interference [15] or dynamic scheduling [16] have been proposed. Finally, Saluja et al. [17] proposed a novel distance-based method with a tunable parameter that adapts to the network traffic. They evaluate the proposed scheme with a stochastic geometry model, and their results outperform the most discussed distance-based schemes in the literature. Also, their algorithm is suitable to LoRaWAN in terms of low computational requirements.

The research of LPWAN in industrial scenarios increased in recent years, especially regarding LoRaWAN. Ballerini et al. [18] presented an experimental analysis of LoRaWAN and NB-IoT (narrow-band IoT, the current 4G/5G LPWAN technology), comparing them on industrial scenarios. The application covers crack measurements in civil structures while they compare the technologies in terms of energy efficiency and coverage. The work shows LoRaWAN as more energy efficient in most scenarios. However, they also show that the energy consumption is almost independent of the payload size. Thus, if the device can aggregate multiple packets into a single transmission (latency tolerant applications), NB-IoT has an advantage. This happens because NB-IoT supports larger payload sizes than LoRaWAN, and then can aggregate more and larger packets. Another industrial potential for LPWANs is energy metering, as shown in [19]. The authors present the impact of sampling strategies that can reduce traffic in LoRaWAN. The possible high traffic is arguably a limiting factor for LoRaWAN, especially for more sensitive industrial applications. Thus, Beltramelli et al. [20] proposed a framework to analyze different access protocols for LoRaWAN, comparing pure-ALOHA with slotted-ALOHA and carrier sense multiple access with collision avoidance (CSMA/CA). The idea is to diminish the interference sensed by devices in dense networks. Their results show that slotted-ALOHA outperforms pure-ALOHA at the cost of energy efficiency and that CSMA outperforms both ALOHA schemes with lower spreading factors (SF) setups but converges to pure-ALOHA with higher SF. This happens because their setup puts higher SF in the outermost part of the network since it uses lower data rates to achieve longer distances. Thus, these devices are more susceptible to the hidden terminal problem. We can see a solution to avoid this problem in [21], where the authors proposed a LoRaWAN range extender through a relay node, suitable for industrial scenarios. The authors perform an experimental campaign to verify the feasibility of the range extender, which indicates promising results and can be extended to different functionalities, as it is transparent and backward compatible with standard LoRaWAN.

Another focus for LPWAN, especially LoRaWAN, is on decoding simultaneous or collided packets. Ben Temim et al. [22] presented an overview of several works that deal with LoRaWAN multiple signal decoding. They state some works did not consider real-world scenario challenges, such as frequency and time synchronization, and interference from signals within the same LoRaWAN SF. Thus, they propose an algorithm that deals with such issues and that can apply SIC to decode multiple superposed signals. On a different approach, Sant'Ana et al. [23] investigated the performance impact of superposed signal decoding on LoRaWAN-like networks. They address cases where only two packets are being transmitted simultaneously, which is the most common collision scenario. Their results show an increase of over two times in the number of served users while keeping the same success probability. Finally, Minhaj et al. [24] extended the previous work investigating the performance of SIC-enabled devices under imperfect orthogonality of LoRa SFs. By using a few well-known SF allocation schemes, the work concludes that the use of SIC-enabled devices is more beneficial on devices closer to the gateway. On a similar research line, Garlisi et al. [25] proposed a new generation of LoRa receivers, able to perform SIC decoding and time synchronization. They evaluate their proposal by implementing the receiver and investigating its performance in the presence of collisions. They conclude that their proposed scheme generates an increase of 50% based on traditional receivers. Multiple simultaneous transmissions are exploited in [26], but the authors considered specific characteristics of LoRaWAN to transmit multiple packets at the same time with different SF. They apply it to a specific channel, where devices may transmit with a higher power.

B. Contributions

In this article, we built upon the LoRa stochastic geometry model from [14], considering that the gateway can decode superposed signals. Different from [26], we are retransmitting previous packets, power multiplexed with the newest one, all of them on the same channel with the same code (if there is any). Also, different from traditional replication schemes in [10], [11], [12], [13], [14], we do not increase the network traffic nor require more transmit power. Instead, the device distributes the transmission power, while keeping a fixed power difference between the replicas. For this, we consider devices can transmit multiple LoRa signals at the same time. In general, our proposal introduces a novel mechanism to increase the reliability of MTC communications based on nonorthogonal multiple access (NOMA) and SIC. Thus, our contributions are summarized as follows.

TABLE I
LIST OF VARIABLES

Variable	Description
$\bar{N}$	Average number of devices
B	Bandwidth
γ	Capture ratio
f_c	Carrier frequency
$\mathcal{V}$	Circular coverage region
p	Device duty cycle
d_k	Device k distance from gateway
h_k	Device k fading
G	Fixed power difference between replicas
no	Index of nonorthogonal replica
V	Network area
ρ	Network device density
R	Network radius
F	Noise figure
σ_w^2	Noise power
M_{no}	Number of nonorthogonal replica
η	Path loss exponent
α	PPP
Φ	Poisson point process
q	Receiver sensitivity
ξ	SIC residual interference ratio
q	SNR threshold
c	Speed of light
$\mathcal{P}_t$	Total transmit power
$\mathcal{P}_{\text{no}}$	Transmit power of replica no
λ	Wavelength

1) A method where each device replicates previous messages by transmitting them superposed with its current transmission by distributing the transmit power level.
2) A generic closed-form approximation that describes the power multiplexed replication scheme, validated by Monte Carlo simulations.
3) An evaluation that considers configuration parameters, such as power allocation, as well as technology parameters, such as residual interference due to imperfect SIC decoding and possible capture ratios.
4) A detailed analysis in terms of success probability and energy efficiency, which shows the prevalence of the proposed method over other replication schemes.

C. Organization

The rest of this article is organized as follows. In Section II we present the network system model. In Section III we discuss the motivation for this work, a specific case and then the general formulation for the proposed scheme, some implementation aspects, and an energy consumption model to evaluate the proposed scheme. Section IV presents numerical results and an analysis of the proposed scheme. Finally, Section V concludes this article. Table I presents a list of the main symbols used in this work.

II. System Model

Following [9], we consider a circular coverage region $\mathcal{V} \subseteq \mathbb{R}^2$ with radius R meters and area $V = \pi R^2$, with $\bar{N}$ devices on average, uniformly deployed, with the gateway at the origin. We assume that the reference[2] node is d_1 meters from the gateway. We model activity in each ring by a homogeneous poisson point process (PPP) Φ with intensity[3] $\alpha = 2p\bar{N}$, $\alpha > 0$, where p is the duty cycle of the nodes.[4] The average number of devices is $\bar{N} = \rho V$, where ρ is the network device density. All devices transmit in the uplink at random using ALOHA, with the same bandwidth B and the same fixed transmit power $\mathcal{P}_t$. An example of a network is shown in Fig. 1, where we have the circular coverage region $\mathcal{V}$. In this network snapshot, we have $N = 1000$ devices on it, where two of them are active (transmitting). Note the gateway at the center of the network.

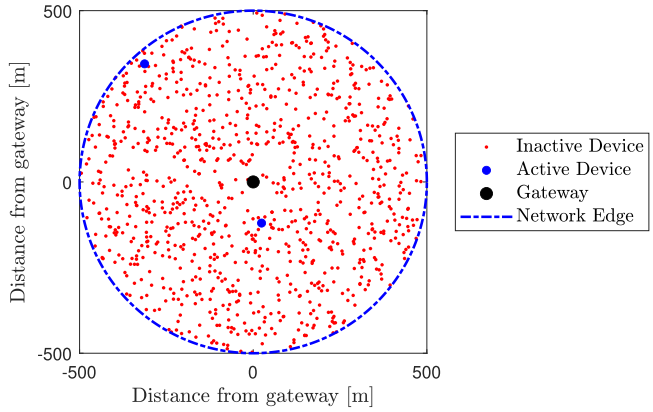

Fig. 1. System model with an example deployment of $N = 1000$ devices, where two of them are active at the given time.

We model path loss as $g_k = (\frac{\lambda}{4\pi})^2 d_k^{-\eta}$, where d_k is the distance from the kth node to the gateway, $\lambda = c/f_c$ is the wavelength, c is the speed of light, f_c is the carrier frequency, and η is the path loss exponent. The model also assumes Rayleigh fading h_k, thus, fading power is exponentially distributed, i.e., $|h_k|^2 \sim \exp(1)$.

If the reference LoRa node transmits the signal s_1, the received signal at the gateway, r_1, is the sum of the attenuated transmitted signal, interference, and noise

$$r_1 = \sqrt{\mathcal{P}_t g_1} h_1 s_1 + \sum_{k \in \phi} \sqrt{\mathcal{P}_t g_k} h_k s_k + w \tag{1}$$

where, $\phi = \Phi \setminus \{1\}$ contains the active nodes in the PPP but the reference node, w is additive white Gaussian noise (AWGN) with zero mean and variance σ_w^2.

A node is in coverage if it is connected to the gateway (probability H_1) and there is no collision (probability Q_1), which considers the signal-to-interference-plus-noise ratio [27]. A collision occurs when simultaneous transmissions use the same SF, and the signal-to-interference ratio (SIR) is below the threshold γ. The coverage probability is [8], [9]

$$C_1 \approx H_1 Q_1. \tag{2}$$

[2]We use subscript "1" to denote the reference device under analysis.
[3]Note that the PPP intensity α in our model translates into a measurement of the traffic generated by the network.
[4]Which is assumed to be twice that of the application in order to consider the use of unslotted-ALOHA.

Using an approximation instead of equality in (2) comes from the fact that (2) assumes independence between the probabilities, which it is a tight approximation [14], considerably simplifying the mathematical formulation.

A. Connection Probability

The connection probability H_1 depends on the distance between a node and the gateway. A node is connected if the signal-to-noise ratio (SNR) at the gateway is above a threshold. The connection probability is $H_1 = \mathbb{P}[\text{SNR} \geq q \mid d_1]$, where q is the SNR reception threshold. Therefore, as the instantaneous $\text{SNR} = \frac{\mathcal{P}_t |h_1|^2 g_1}{\sigma_w^2}$, and assuming Rayleigh fading, H_1 is

$$H_1 = \mathbb{P}\left[|h_1|^2 \geq \frac{\sigma_w^2 q}{\mathcal{P}_t g_1} \,\middle|\, d_1\right] = \exp\left(-\frac{\sigma_w^2 q}{\mathcal{P}_t g_1}\right). \tag{3}$$

B. Capture Probability

As in [9], we model the SIR as

$$\text{SIR} = \frac{\mathcal{P}_t |h_1|^2 g_1}{\sum_{k\in\phi} \mathcal{P}_t |h_k|^2 g_k} = \frac{|h_1|^2 d_1^{-\eta}}{\sum_{k\in\phi} |h_k|^2 d_k^{-\eta}}. \tag{4}$$

The probability of successful reception in the presence of interference, considering the capture effect, is

$$Q_1 = \mathbb{P}\left[\text{SIR} \geq \gamma \mid d_1\right] \tag{5}$$

where, γ is the capture threshold. As detailed in [9], [11], we can reduce Q_1 applied to our model as

$$Q_1 = \exp\left[-\alpha_2 F_1\left(1, \frac{2}{\eta}; 1 + \frac{2}{\eta}; \frac{R^{-\eta}}{\gamma d_1^{\eta}}\right)\right] \tag{6}$$

where, ${}_2F_1(\cdot)$ is the Gauss hypergeometric function [28]. See the proof in Appendix A for $X = Z$ and $Y = 0$. The definitions of these parameters are found in the appendix.

III. Nonorthogonal Replication Scheme

A. Motivation

Packet independent replication, as presented in [13], is the most efficient replication scheme compared to embedded approaches, where in the latter redundant information is attached to the same packet containing original information. Replicas in the independent scheme perceive different channel realizations, generating diversity gain, whereas, in the embedded model, we always have a replica with the same channel realization of the original transmissions. In exchange for that, independent replication generates extra traffic because of overhead coming from multiple transmissions. On the other hand, embedded schemes yield longer transmissions if we consider a fixed transmission rate. Moreover, we can see that, due to the high link budget and a large number of users, collisions are often the most limiting factor for LPWANs reliability, especially with independent replications [11]. Thus, also motivated by recent works on detection and decoding of multiple signals in LPWANs [22], [25], we propose a nonorthogonal power multiplexed replication scheme that exploits the large available link budget, splitting the transmit power into multiple transmissions from a given node at the same time slot. Finally, the approach does not increase the network traffic, so that it can be combined with other independent replication schemes.

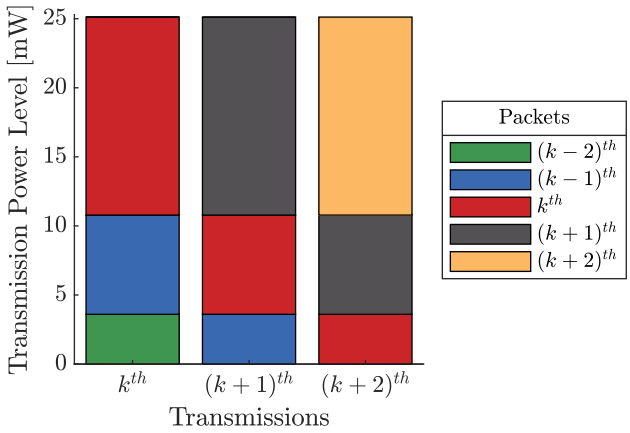

Fig. 2. Representation of the power allocation throughout packets on nonorthogonal replication with $M_{\text{no}} = 3$, $P_t = 14$ dBm $\approx$ 25.1 mW, $G = 3$ dB, and $\xi = 0$.

Inspired by the coding methods in [13], consider that a device a wants to transmit the kth information packet. Then, to increase the reliability of this transmission, a replicates this message M_{no} times (suffix no from nonorthogonal). However, instead of attaching the redundant information on the next transmission (RT-E) or transmitting it as a new packet (RT-I), the redundant message is power-multiplexed with the next $M_{\text{no}} - 1$ transmissions. Thus, we have that each transmission from device a is a multiplexing of M_{no} messages.

Prior to transmission, a must allocate different power levels for each multiplexed message. For simplicity, we assume a fixed power ratio G between messages, where $G > \gamma$, recalling that γ is the capture threshold. Then, applying an SIC decoding method, the receiver tries to decode the received messages inside a packet, from the stronger to the weaker. One disadvantage of this replication scheme is an increased delay compared to RT, as the receiver would need to await a new transmission to recover a lost message. This disadvantage is also present in the coded and hybrid schemes, where the receiver needs future coded messages to recover past lost packets. This is most detrimental in applications with long periods between transmissions. However, when consecutive transmissions are separated by a few minutes, this will only affect very high freshness demanding applications.

An example of three consecutive transmissions from the same device using the nonorthogonal scheme is presented in Fig. 2. Here, each color represents the same packet, which is replicated $M_{\text{no}} = 3$ times, and which is also the number of multiplexed packets per transmission. Note that the power difference $G = 3$ dB is on the logarithmic scale. We can see at the kth transmission that the kth packet, which is the newest, is being transmitted with a higher power. The two previous packets, $(k-1)$th and $(k-2)$th are transmitted with lower power. In the $(k+1)$th transmission, the kth packet is transmitted with lower power, since the $(k+1)$th packet is the newest now. Finally, at the $(k+2)$th transmission, the kth packet is transmitted at the lowest power level, which is its last replica.

B. Two-Packets Nonorthogonal Replication

First, we consider a two-packet replication, the simplest configuration. It means that, for each duty cycle, we transmit the kth packet power multiplexed with a replica of the previous packet, $(k-1)$th, with respectively transmit powers $\mathcal{P}_i$ and $\mathcal{P}_j$, where the total transmit power is $\mathcal{P}_t = \mathcal{P}_i + \mathcal{P}_j$. Moreover, considering $\gamma > 1$, the SIR threshold to decode a packet in the presence of interference, and a given $0 \leq \xi \leq 1$ interference residue due to imperfect SIC, the transmit powers must follow:

$$\gamma\xi\mathcal{P}_i < \mathcal{P}_j < \frac{\mathcal{P}_i}{\gamma}, \quad \forall\, \xi < \frac{1}{\gamma^2}. \tag{7}$$

Note that, for the kth message to be successfully decoded by the gateway, despite the interference of the $(k-1)$th message, P_i has to be at least γ times stronger than P_j. Whereas, P_j has to be at least γ times stronger than the residual interference from the imperfect SIC, given by ξP_i, to ensure that the $(k-1)$th message is decoded by the gateway after removing the kth message. Note that there is a relation between ξ and γ since $\xi\gamma\mathcal{P}_i < \frac{\mathcal{P}_i}{\gamma}$. This implies that worse SIC interference residue may require lower SIR thresholds and vice versa. The scenario for power allocation becomes more strict as γ and ξ grow. Thus, a first insight we have is that better signal detection and SIC decoding methods result in more power allocation possibilities. Note that the same insight applies not only to the case of two-packet replication but to other cases, too.

1) Connection Probabilities: The connection probability of packet i follows the same steps as in (3), but using P_i as the transmit power. In order to receive packet j, we must receive packet i first. Since their SNR are related through h_1 and d_1, we cannot consider them as independent. So, the connection probability for packet j is

$$H_j = \mathbb{P}[\text{SNR}_j \geq q, \text{SNR}_i \geq q | d_1]. \tag{8}$$

However, $\mathcal{P}_i > \mathcal{P}_j$ and both messages suffer from the same channel gain $|h_1|^2 g_1$. Thus, we always have that $\text{SNR}_i > \text{SNR}_j$. Finally

$$H_j = \mathbb{P}\left[\text{SNR}_j \geq q | \, d_1\right] = \exp\left(-\frac{\sigma_w^2 q}{\mathcal{P}_j g_1}\right). \tag{9}$$

2) Capture Probabilities: Here, we have two different capture probabilities for each packet, each one with its own SIR.

First, we start with packet i. Thus, we are decoding the strongest message i in the presence of the weakest message j and possible external interference. Following Appendix A, with $X = P_i, Y = P_j$, and $Z = P_t$, the capture probability of packet i is

$$Q_i = \exp\left[-\alpha_2 F_1\left(1, \frac{2}{\eta}; 1 + \frac{2}{\eta}; -\frac{\mathcal{P}_i - \gamma\mathcal{P}_j}{\gamma\mathcal{P}_t R^{-\eta} d_1^{\eta}}\right)\right]. \tag{10}$$

Now, we are considering the case that the message of interest is the replica transmitted as packet j. In practice, the gateway first decodes packet i, remove it from the received signal, and then tries to decode packet j. Note that we might consider that packet i is not completely removed from the received signal, with a residual interference fraction ξ, because of nonoptimal SIC performance. The probability that packet j is received depends on Q_i due to h_1 and d_1, and thus the SIR from both packets i and j must be above the threshold γ as

$$Q_j = \mathbb{P}\left[\text{SIR}_j > \gamma, \ \text{SIR}_i > \gamma \mid d_1\right]. \tag{11}$$

Moreover, we can assume an approximation for (11), termed as Q_j^*, considering that $\text{SIR}_j < \text{SIR}_i$ for practical values of ξ, G, and that there is always the presence of some interference. Thus, we can approximate (11) as

$$Q_j^* = \mathbb{P}\left[\text{SIR}_j > \gamma \mid d_1\right]. \tag{12}$$

Following Appendix A, with $X = P_j$, $Y = \xi P_i$, and $Z = P_t$, the capture probability of packet j is

$$Q_j^* = \exp\left[-\alpha_2 F_1\left(1, \frac{2}{\eta}; 1 + \frac{2}{\eta}; -\frac{\mathcal{P}_j - \xi\gamma\mathcal{P}_i}{\gamma\mathcal{P}_t R^{-\eta} d_1^{\eta}}\right)\right]. \tag{13}$$

3) Coverage Probability: The total coverage probability is

$$C_2 \approx H_i Q_i + (1 - H_i Q_i) H_j Q_j^* \tag{14}$$

which considers the probability of decoding the information as the strongest packet (subscript i), and, in case of failure, the probability of acquiring it as the weakest packet (subscript j).

C. General Equations

Extending the analysis from the previous sections, we can generalize the nonorthogonal replication equations for any number of replicas M_{no}. First, we can derive the connection probability straightforward from (3) as

$$H_{\text{no}} = \mathbb{P}\left[|h_1|^2 \geq \frac{\sigma_w^2 q}{\mathcal{P}_{\text{no}} g_1} \,\middle|\, d_1\right] = \exp\left(-\frac{\sigma_w^2 q}{\mathcal{P}_{\text{no}} g_1}\right) \tag{15}$$

where, $\mathcal{P}_{\text{no}}$ is the transmit power for packet no $\in \{1, 2, \ldots, M_{\text{no}}\}$ within each nonorthogonal power multiplexed transmission.

To follow the procedure in Appendix A and find the capture probability, we must define the self-interference with M_{no} multiplexed replicas. We can separate it into two parts. The first with the stronger packets that were already decoded and removed from the received signal, from 1st to the $(\text{no}-1)$th packet. These terms will contribute multiplied by ξ, considering imperfect SIC at the reception. The second part contains the weaker packets that are still present in the decoded packet, $(\text{no}+1)$th to (M_{no})th, and fully contribute to the interference. Thus, we can define the self-interference generated by other multiplexed messages to the noth message on a M_{no} replication scheme as

$$\mathcal{Z}_{\text{no}} = \left(\xi \sum_{a=1}^{\text{no}-1} P_a + \sum_{b=\text{no}+1}^{M_{\text{no}}} P_b\right). \tag{16}$$

Similar to (10) and (13), following Appendix A with $X = P_{\text{no}}$, $Y = \mathcal{Z}_{\text{no}}$ and $Z = P_t$, we have the general nonorthogonal capture probability

$$Q_{\text{no}}^* = \exp\left[-\alpha_2 F_1\left(1, \frac{2}{\eta}; 1 + \frac{2}{\eta}; -\frac{\mathcal{P}_{\text{no}} - \gamma\mathcal{Z}_{\text{no}}}{\gamma\mathcal{P}_t R^{-\eta} d_1^{\eta}}\right)\right]. \tag{17}$$

Finally, by expanding (14) for M_{no} nonorthogonal replications, the coverage probability is

$$C_{M_{\text{no}}} \approx \sum_{a=1}^{M_{\text{no}}} \left[H_a Q_a^* \left(\prod_{b=1}^{a-1} 1 - H_b Q_b^* \right) \right]. \tag{18}$$

Note that (18) depends not only on the number of nonorthogonal power multiplexed replications M_{no}, but also on the transmit power levels for each replica. As stated before, a bad configuration might lead to worse performance. The transmit power levels for each message must follow:

$$\mathcal{P}_{\text{no}} > \gamma \mathcal{Z}_{\text{no}} \; \forall \; \text{no} \in \{1, 2, \ldots, M_{\text{no}}\} \tag{19}$$

where, we recall $\mathcal{Z}_{\text{no}}$ is the amount of self-interference generated by all multiplexed messages to the noth message. The abovementioned can be obtained by expanding the logic in (7), where now we account for all M_{no} multiplexed messages. Here, the power multiplexed message the gateway is decoding must be γ times stronger than the weaker multiplexed messages plus the residue from those already decoded. When (19) is not satisfied, we have multiplexed messages that will never be decoded due to self-interference. Moreover, it leads to nonnegative numbers on the last term of the ${}_2F_1(\cdot)$ function in (17), presenting undesired behaviors, like complex results. Different from (7), we could not find a closed-form equation to represent the transmit power levels as a function of M_{no}, because of the excessive algebraic complexity. Thus, we numerically derive valid transmit power levels for a fixed G. We discuss this procedure in Section IV.

D. Implementation Considerations

The proposed scenario is an uplink NOMA, but with superposed messages being transmitted by the same device. Thus, it resembles more downlink NOMA than typical uplink NOMA. Note that this scenario is much simpler than what it is usually required for NOMA in IoT, like time and frequency synchronization [22], [25], [29] and power control [30], where the superposed messages come from different devices.

Moreover, one of the messages was generated at the transmission time, but the replicas were generated previously. Thus, the device needs a memory buffer to store this information, which increases with the size and number of messages. Finally, it might be interesting for the receiver to know some parameters, such as the number of superposed messages and the power difference between them. The exchange of these parameters could be easily done when devices enter the network.

The combination of signals could follow similarly as in [29], but with the same modulation configurations for all transmissions. The device generates the signals in baseband, for example, CSS and DBPSK/GFSK for LoRa and Sigfox, respectively, and adds the signals considering the specific power allocation among them. Next, the device upconverts the summed signals to transmit in passband.

Another concern is on decoding the superposed signals, which means applying SIC at the receiver. The authors in [22] and [25] presented an enhanced receiver to decode LoRa-like signals that come from different sources. Both works do not require perfect frequency and time synchronization. The work in [31] proposed a SIC algorithm for LTE interference in NB-IoT systems, using M-QAM and QPSK, respectively, and implements it using a test kit. As far as our knowledge is concerned, we did not find any work regarding SIC on the ultranarrowband scheme adopted by Sigfox. However, it uses well-known modulations, and thus, it should not be an issue.

E. Energy Consumption

Just like system reliability, the energy consumption of an IoT device is an important performance indicator. In traditional message replication schemes, we are tradingoff power consumption to improve reliability. Thus, it is contradictory to consider these methods energy efficient. In contrast, the proposed nonorthogonal scheme, as discussed in Section III-D, can consume the same amount of energy as a regular transmission. This means we can increase the system reliability without increasing energy utilization.

To address and compare the energy consumption, we use the model first presented in [32] for LoRa networks. The model considers eleven different states, where each state has its current consumption and, when combined, represent the total energy consumption between two transmissions, including the sleeping period.

Moreover, we use the same protocol for replication schemes presented in [14], as well as the same duration and current values. The protocol considers that devices always open a single receiving window after transmitting a message, disregarding the number of replicas. This reduces the amount of energy spent by these schemes, and we judge it as the fairest way to compare traditional replication methods. Thus, the average current consumption to transmit one message is

$$I_{\text{avg2}} = \frac{M}{P} \left(\sum_{i=1}^{N_{\text{states}}-5} T_i I_i + \sum_{i=7}^{N_{\text{states}}-1} T_i I_i + T_{\text{sleep2}} I_{\text{sleep}} \right) \tag{20}$$

where, T_{sleep2} is the sleep duration

$$T_{\text{sleep2}} = P - M \sum_{i=1}^{N_{\text{states}}-5} T_i - \sum_{i=7}^{N_{\text{states}}-1} T_i. \tag{21}$$

Note that M varies for other replication methods, but $M = 1$ for all configurations of the proposed scheme. Finally, the energy per packet transmission, which means the energy a device spends within one transmission period, is

$$\mathcal{E} = P I_{\text{avg2}} V_{\text{dc}}. \tag{22}$$

The power consumption model has been intended solely to establish a fair comparison according to that performance metric. For a better understanding on the model details, we recommend the readers to check [32] and [14].

IV. Numerical Results

In this section, we evaluate the proposed scheme in terms of reliability and some of its features. Unless stated otherwise,

TABLE II
PARAMETERS USED IN THE NUMERICAL RESULTS

Parameter	Value
Average number of devices $\bar{N}$	10^3
AWGN power	-117 dBm
Bandwidth B	125 kHz
Capture ratio γ	1 dB [34]
Carrier frequency f_c	868 MHz
Duty cycle p	$41.22/(3 \times 10^5)$
Message period P	300 s
Network radius R	500 m
Noise figure F	6 dB
Path-loss exponent η	2.8
Reference device distance to the gateway d_1	500 m
SIC residue imperfection ξ	0
SNR threshold q	-6 dB
Power difference between levels G	3 dB
Time-on-air	41.22 ms
Transmit power P_t	14 dBm
Dc voltage V_{dc}	3.3 V

TABLE III
TRANSMIT POWER LEVELS IN MW FOR DIFFERENT NUMBER OF REPLICAS M_{NO} AND POWER DIFFERENCE BETWEEN LEVELS G, CONSIDERING A TOTAL TRANSMIT POWER OF 25.1 MW

Number of replicas M_{no}	Power difference G 3 **dB**	6 **dB**
1	[25.1] mW	[25.1] mW
2	[16.7, 8.4] mW	[20.1, 5.0] mW
3	[14.3, 7.2, 3.6] mW	[19.1, 4.8, 1.2] mW

we use the parameters[5] in Table II, which are the same for LoRa technology [33] to transmit a message with nine bytes of payload using spreading factor 7 (SF7). Table III indicates a few examples of power allocation used in the numerical results. We consider different fixed G for all levels and different number of replicas M_{no}. Note that, in the case with three replicas, even when $G = 3$ dB we see that the oldest packet will be transmitted with very low power compared to the others. The value goes even lower with higher G. Thus, this is an insight that $M_{\text{no}} > 2$ produces very interference-sensitive schemes, even with high-performing SIC and favorable capture ratio. None of the $M_{\text{no}} = 3$ configurations are possible for $\xi \geq 0.2$ and $\gamma \geq 1$ dB, since they break the constraint in (19). Also, for all figures in this section, except Fig. 3, we considered $d_1 = R = 500$ m. Similar to [14], this is done to enable us to consider the network traffic by increasing the number of users, while we consider the worst-case scenario device at the network edge. Finally, for all figures in this section, except Fig. 7, markers are Monte Carlo simulations, where each point is the averaged result of 10^5 random deployment scenarios. The solid lines represent analytical results, each one generated with the equations presented in Section III.

In Fig. 3, we plot the different success probabilities derived in Section III. We recall that H_i, H_j, Q_i, and Q_j^* represent

[5]The considered value for duty cycle p is equivalent to one packet of 41.22 ms long each 5 min.

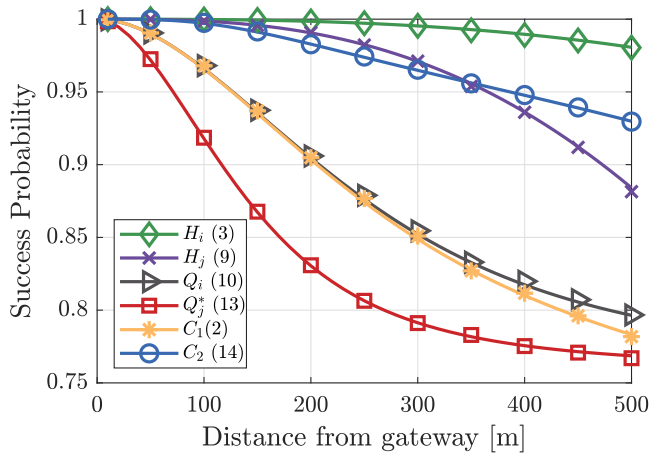

Fig. 3. Analytic and Monte Carlo simulation success probabilities as a function of the distance from the gateway.

the connection and capture probabilities of packets i and j, respectively, while C_1 and C_2 are the coverage probability of conventional transmission and the proposed scheme with $M_{\text{no}} = 2$ replicas, respectively. Note that the numbers next to the probabilities symbols in the legend refer to the equations of each probability in this article. We also recall that Q_i and Q_j^* can be obtained by (17), while C_1 and C_2 by (18) with the proper parameters. Here, we investigate the accuracy of these probabilities. We can see that the simulations match the analytical results very well. In particular, (13) in red, proved to be a good approximation, as the simulation, in red squares, matched the analytical results. We can see the expected behavior of the success probability decaying with the distance, as devices further from the gateway suffer more from the path loss, and thus, will have lower connection and capture probabilities. We can see that H_i and Q_i are always greater than H_j and Q_j^*, which makes sense, since $\mathcal{P}_i > \mathcal{P}_j$. Moreover, we can see that the proposed scheme, in blue, outperforms the conventional scheme, in yellow. This gap is larger for devices at the network border, which highlights the benefit of our proposed scheme in increasing the worst-case reliability. Finally, the results in blue can be obtained either by (14) or (18), with $M_{\text{no}} = 2$.

Fig. 4 compares the proposed nonorthogonal scheme with the simplest replication method in the literature (RT-I), where a device transmits the same message m times in terms of success probability versus the average number of devices. We can see the RT-I success probability curves present a greater slope as $\bar{N}$ increases. This is due to the increased amount of traffic from the RT-I replications, where the traffic is multiplied by m. The nonreplication scheme suffers less from the increased amount of devices. The result of the nonorthogonal replication outperforming RT-I is case-specific. However, it is clear that with the increase in the number of devices, nonorthogonal replications become more appealing.

Fig. 5 depicts traditional and nonorthogonal replication success probabilities as a function of the average number of devices. We compare the regular LoRa C_1, i.e., with no replications, with the proposed nonorthogonal scheme with $M_{\text{no}} = 2$ and 3, C_2 and

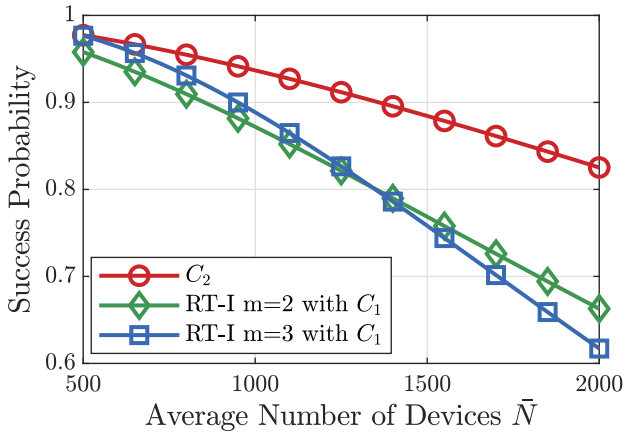

Fig. 4. Success probability of the nonorthogonal replication (C_2) and the independent replication transmission (RT-I) [11], [13] with different number of replicas, as a function of the average number of users.

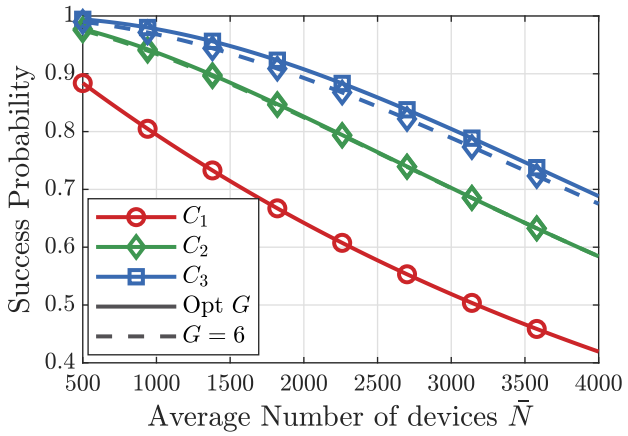

Fig. 5. Analytic traditional (C_1) and nonorthogonal replication (C_2 and C_3) LoRa success probabilities as a function of the average number of devices.

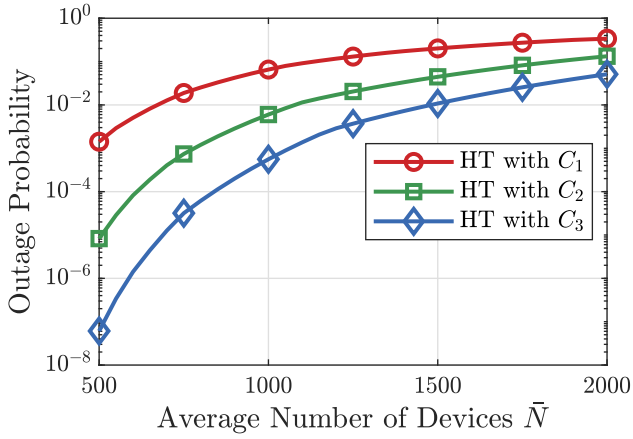

Fig. 6. Outage probability of the HT replication in [14] when merged with the proposed power multiplexing scheme, for a different number of nonorthogonal replications, as a function of the average number of users.

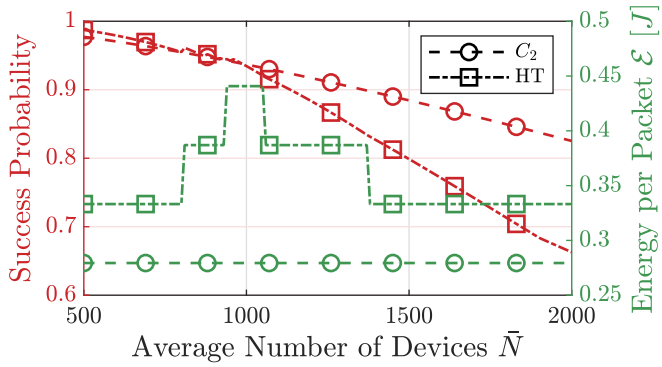

Fig. 7. Success probability and energy per packet for C_2 and HT schemes for different average number of devices.

C_3, respectively. We can see the gain that nonorthogonal power multiplexed replicas bring to the success probability. Also, we consider the impact of optimal G against a fixed G for both C_2 and C_3. We considered fixed $G = 6$ dB as a naive guess, since optimal values tend to be lower for $\gamma = 1$, but it is still a valid parameter value for this scenario. We can see again that optimizing G may not bring a large gain in terms of performance for C_3, being almost negligible for C_2. However, similar to what was concluded before for ξ and γ, the choice of G can limit the parameter selection, and thus it should be carefully chosen based on the receiver decoding parameters.

Unlike the previous analysis, in Fig. 6 we plot the outage probability for the traditional and nonorthogonal replication schemes, but now operating with the optimized hybrid transmission (HT) scheme. Note that the nonorthogonal proposed scheme can be combined with other independent replication methods, as that known as HT and introduced in [14]. We applied exhaustive search optimization and considered the same conditions for all devices in the network. This is done by selecting a finite number of configurations that do not exceed ten replications per message. Then, we test all replication configurations for each average number of users and select the best performing. The results are shown in Fig. 6. Since the success probability goes close to 1, we show the outage probability $(1 - C_{M_{\text{no}}})$, which allows for obtaining better insights. We can see a gap between using only HT from [14] to when we apply it with the proposed scheme. Increasing the number of nonorthogonal replications (from one to three in the figure) considerably improves the outage probability, indicating the large impact of the proposed method when applied to other state-of-the-art techniques. For example, the outage probability for C_1 (i.e., without the proposed scheme) with 750 devices is achieved with 1250 and 1750 devices for C_2 and C_3, respectively, improving the network capacity.

Fig. 7 depicts the energy consumption of the proposed scheme versus HT. Here, we consider $M_{\text{no}} = 2$ for the nonorthogonal scheme. It is normal that the success probability with optimal HT presents a higher energy consumption. Notice that HT will always consume more energy than the proposed scheme, due to more transmissions. The proposed scheme, on the other hand, will split the power budget to transmit messages simultaneously, leading to consumption equivalent to no replication. So, we optimize HT to match the nonorthogonal success probability, while using the least energy consumption configuration. From

$800 \leq \hat{N} \leq 1000$ we see HT increasing the number of replicas to match C_2 success probability. At around $\hat{N} \geq 1000$, HT cannot keep with the nonorthogonal method. So, we consider HT using the optimal success probability configuration, disregarding its energy consumption. We can see that HT can get the same success probability as the proposed scheme with a smaller number of devices, at a larger energy cost. With a larger number of devices, the proposed scheme outperforms HT, while using at least 17% less energy. Note that this energy comprises the consumption of transmission and sleep states until the next transmission. Thus, with a smaller period, which means, more transmissions, this percentage could increase.

V. Conclusion

In this article, we proposed a novel power multiplexing replication scheme for LPWANs and evaluated it in a generic IoT application scenario. Unlike previous works, the proposed scheme does not increase network traffic, being more appropriate for random access networks as it does not increase the collision probability. We analyzed the proposed scheme for different configurations, evaluating the impact of imperfect SIC at the receiver and concluding that the system is robust. We also investigated the use of the proposed scheme with previous independent replication methods from the literature. Finally, we show that traditional replication schemes use more energy per packet to achieve the same reliability as the proposed method. This energy consumption increases with network traffic, thus deteriorating the performance of the other replication methods compared to the method proposed here. The results are promising, showing that the proposed method increases the capacity of LPWANs.

Appendix A
Derivation Steps of Capture Probabilities

A. Derivations Concerning Q_1 (6) Q_i (10), Q_j^* (13), and Q_{no} (17)

Following similar steps as in [14], we formulate a general derivation of the capture probabilities. Without loss of generality, let us consider a general SIR as

$$\text{SIR}_x = \frac{X|h_1|^2 d_1^{-\eta}}{Y|h_1|^2 d_1^{-\eta} + Z\sum_{k\in\phi}|h_k|^2 d_k^{-\eta}} \tag{23}$$

where, X represents the reference packet transmission power, Y is the self-interference power, i.e., interference from different packets on the same transmission, and Z is the average power of the interference from other simultaneous transmissions. Let h be Rayleigh fading component, η the path loss exponent, while d the distance from the device to the gateway, which is uniformly distributed over the circular area of radius R.

For a packet to be successfully decoded in the presence of interference, its received power must be γ times stronger than the interference, which means the SIR must be higher than γ. Thus, the capture probability can be written as

$$Q_x = \mathbb{P}\left[\text{SIR}_x \geq \gamma \mid d_1\right]. \tag{24}$$

Substituting (23) on (24) and applying some simplifications, we have that

$$Q_x = \mathbb{P}\left(|h_1|^2 > \frac{\gamma Z d_1^{\eta}\sum_{k\in\phi}|h_k|^2 d_k^{-\eta}}{X-\gamma Y} \;\middle|\; d_1\right). \tag{25}$$

Recalling that $|h_1|^2$ and $|h_k|^2$ follow an exponential distribution of unitary mean and have no correlation, we have that

$$\begin{aligned} Q_x &= \mathbb{E}_{|h_k|^2,\phi}\left[\prod_{k\in\phi}\exp\left(-\frac{\gamma Z d_1^{\eta}|h_k|^2 d_k^{-\eta}}{X-\gamma Y}\right)\right] \\ &= \mathbb{E}_{\phi}\left[\prod_{k\in\phi}\frac{X-\gamma Y}{X-\gamma Y+\gamma Z d_k^{-\eta} d_1^{\eta}}\right] \end{aligned} \tag{26}$$

where, $\phi = \Phi \setminus \{1\}$ contains the active nodes in the PPP but the reference node.

Then, using the probability generating functional of the product over PPPs

$$\mathbb{E}\left[\prod_{x\in\phi} f(x)\right] = \exp\left(-\beta\int_{R^2} 1 - f(x)\,\mathrm{d}x\right) \tag{27}$$

where, $\beta = 2p\rho$ is multiplied by 2 to approximate unslotted ALOHA, and converting it to polar coordinates, we have that

$$Q_x = \exp\left(-4\pi p\rho\int_0^R \frac{\gamma d_k^{-\eta} d_1^{\eta} Z}{X-\gamma Y+\gamma Z d_k^{-\eta} d_1^{\eta}} d_k\, d d_k\right). \tag{28}$$

The previous internal integral can be written as a Gauss hypergeometric function [28], giving

$$Q_x = \exp\left[-\alpha_2 F_1\left(1, \frac{2}{\eta}; 1+\frac{2}{\eta}; \frac{R^{\eta}(\gamma Y - X)}{d_1^{\eta}\gamma Z}\right)\right] \tag{29}$$

recalling that $\alpha = 2p\bar{N}$ is the PPP density, $\bar{N} = \rho V$ is the average number of devices and $V = \pi R^2$ is the network area.

References

[1] L. Chettri and R. Bera, "A comprehensive survey on Internet of Things (IoT) toward 5G wireless systems," *IEEE Internet Things J.*, vol. 7, no. 1, pp. 16–32, Jan. 2020.

[2] N. H. Mahmood et al., "Machine type communications: Key drivers and enablers towards the 6G era," *EURASIP J. Wireless Commun. Netw.*, vol. 2021, no. 1, Jun. 2021.

[3] M. Vaezi et al., "Cellular, wide-area, and non-terrestrial IoT: A survey on 5G advances and the road towards 6G," *IEEE Commun. Surveys Tuts.*, vol. 24, no. 2, pp. 1117–1174, Apr.–Jun. 2022.

[4] M. A. Ullah, K. Mikhaylov, and H. Alves, "Enabling mMTC in remote areas: LoRaWAN and LEO satellite integration for offshore wind farm monitoring," *IEEE Trans. Ind. Informat.*, vol. 18, no. 6, pp. 3744–3753, Jun. 2022.

[5] O. L. A. López and H. Alves, *Wireless RF Energy Transfer in the Massive IoT Era: Towards Sustainable Zero-Energy Networks*. Hoboken, NJ, USA: Wiley, Nov. 2021.

[6] C. Milarokostas, D. Tsolkas, N. Passas, and L. Merakos, "A comprehensive study on LPWANs with a focus on the potential of LoRa/LoRaWAN systems," *IEEE Commun. Surveys Tuts.*, vol. 25, no. 1, pp. 825–867, Jan.–Mar. 2022.

[7] H. Zhu et al., "Index of low-power wide area networks: A ranking solution toward best practice," *IEEE Commun. Mag.*, vol. 59, no. 4, pp. 139–144, Apr. 2021.

[8] O. Georgiou and U. Raza, "Low power wide area network analysis: Can LoRa scale?," *IEEE Wireless Commun. Lett.*, vol. 6, no. 2, pp. 162–165, Apr. 2017.
[9] A. Mahmood, E. Sisinni, L. Guntupalli, R. Rondón, S. A. Hassan, and M. Gidlund, "Scalability analysis of a LoRa network under imperfect orthogonality," *IEEE Trans. Ind. Informat.*, vol. 15, no. 3, pp. 1425–1436, Mar. 2019.
[10] Y. Mo, M. -T. Do, C. Goursaud, and J.- M. Gorce, "Optimization of the predefined number of replications in a ultra narrow band based IoT network," in *Proc. IEEE Wireless Days*, 2016, pp. 1–6.
[11] A. Hoeller, R. D. Souza, O. L. Alcaraz López, H. Alves, M. de Noronha Neto, and G. Brante, "Analysis and performance optimization of LoRa networks with time and antenna diversity," *IEEE Access*, vol. 6, pp. 32820–32829, 2018.
[12] P. J. Marcelis, V. S. Rao, and R. V. Prasad, "DaRe: Data recovery through application layer coding for LoRaWAN," in *Proc. IEEE/ACM 2nd Int. Conf. Internet Things Des. Implementation*, 2017, pp. 97–108.
[13] S. Montejo-Sánchez, C. A. Azurdia-Meza, R. D. Souza, E. M. G. Fernandez, I. Soto, and A. Hoeller, "Coded redundant message transmission schemes for low-power wide area IoT applications," *IEEE Wireless Commun Lett.*, vol. 8, no. 2, pp. 584–587, Apr. 2019.
[14] J. M. S. Sant'Ana, A. Hoeller, R. D. Souza, S. Montejo-Sánchez, H. Alves, and M. d. Noronha- Neto, "Hybrid coded replication in LoRa networks," *IEEE Trans. Ind. Informat.*, vol. 16, no. 8, pp. 5577–5585, Aug. 2020.
[15] A. Farhad, D.-H. Kim, P. Sthapit, and J. -Y. Pyun, "Interference-aware spreading factor assignment scheme for the massive LoRaWAN network," in *Proc. Int. Conf. Electron., Inf., Commun.*, 2019, pp. 1–2.
[16] B. Reynders, Q. Wang, P. Tuset-Peiro, X. Vilajosana, and S. Pollin, "Improving reliability and scalability of LoRaWANs through lightweight scheduling," *IEEE Internet Things J.*, vol. 5, no. 3, pp. 1830–1842, Jun. 2018.
[17] D. Saluja, R. Singh, S. Gautam, and S. Kumar, "EWS: Exponential windowing scheme to improve LoRa scalability," *IEEE Trans. Ind. Informat.*, vol. 18, no. 1, pp. 252–265, Jan. 2022.
[18] M. Ballerini, T. Polonelli, D. Brunelli, M. Magno, and L. Benini, "NB-IoT versus LoRaWAN: An experimental evaluation for industrial applications," *IEEE Trans. Ind. Informat.*, vol. 16, no. 12, pp. 7802–7811, Dec. 2020.
[19] M. de CastroTomé, P. H. J. Nardelli, and H. Alves, "Long-range low-power wireless networks and sampling strategies in electricity metering," *IEEE Trans. Ind. Electron.*, vol. 66, no. 2, pp. 1629–1637, Feb. 2019.
[20] L. Beltramelli, A. Mahmood, P. Österberg, and M. Gidlund, "LoRa beyond ALOHA: An investigation of alternative random access protocols," *IEEE Trans. Ind. Informat.*, vol. 17, no. 5, pp. 3544–3554, May 2021.
[21] E. Sisinni et al., "LoRaWAN range extender for industrial IoT," *IEEE Trans. Ind. Informat.*, vol. 16, no. 8, pp. 5607–5616, Aug. 2020.
[22] M. A. Ben Temim, G. Ferré, B. Laporte-Fauret, D. Dallet, B. Minger, and L. Fuché, "An enhanced receiver to decode superposed LoRa-like signals," *IEEE Internet Things J.*, vol. 7, no. 8, pp. 7419–7431, Aug. 2020.
[23] J. M. S. Sant'Ana, A. Hoeller, R. D. Souza, H. Alves, and S. Montejo-Sánchez, "LoRa performance analysis with superposed signal decoding," *IEEE Wireless Commun. Lett.*, vol. 9, no. 11, pp. 1865–1868, Nov. 2020.
[24] S. U. Minhaj, S. H. Ali, M. T. Bhatti, S. A. Hassan, A. Mahmood, and M. Gidlund, "How SIC-enabled LoRa fares under imperfect orthogonality?," in *Proc. Int. Wireless Commun. Mobile Comput.*, 2021, pp. 729–734.
[25] D. Garlisi, S. Mangione, F. Giuliano, D. Croce, G. Garbo, and I. Tinnirello, "Interference cancellation for LoRa gateways and impact on network capacity," *IEEE Access*, vol. 9, pp. 128133–128146, 2021.
[26] M. Centenaro and L. Vangelista, "Boosting network capacity in LoRaWAN through time-power multiplexing," in *Proc. IEEE 29th Annu. Int. Symp. Pers., Indoor Mobile Radio Commun.*, 2018, pp. 1–6.
[27] M. Haenggi, *Stochastic Geometry for Wireless Networks*. New York, NY, USA: Cambridge Univ. Press, 2012.
[28] A. Daalhuis, "Hypergeometric function," in *NIST Handbook of Mathematical Functions*. New York, NY, USA: Cambridge Univ. Press, 2010, ch. 15.
[29] Y. Qi, X. Zhang, and M. Vaezi, "Over-the-air implementation of NOMA: New experiments and future directions," *IEEE Access*, vol. 9, pp. 135828–135844, 2021.
[30] W. Cui, C. Liu, W. Yang, and L. Cai, "I-Talk: Reliable and practical superimposed signal decoding without power control," *IEEE Trans. Wireless Commun.*, vol. 20, no. 7, pp. 4269–4281, Jul. 2021.
[31] G. J. González, F. H. Gregorio, and J. Cousseau, "Successive interference cancellation for the NB-IoT uplink multiple access," in *Proc. Argentine Conf. Electron.*, 2020, pp. 41–46.
[32] L. Casals et al., "Modeling the energy performance of LoRaWAN," *Sensors*, vol. 17, no. 10, 2017, Art. no. 2364.
[33] *SX1272/73-860 MHz to 1020 MHz Low Power Long Range Transceiver*, Camarillo, CA, USA: Semtech Corporation, Mar. 2017.
[34] D. Croce, M. Gucciardo, S. Mangione, G. Santaromita, and I. Tinnirello, "Impact of LoRa imperfect orthogonality: Analysis of link-level performance," *IEEE Commun. Lett.*, vol. 22, no. 4, pp. 796–799, Apr. 2018.

Jean Michel de Souza Sant'Ana (Student Member, IEEE) received the B.Sc. degree in telecommunications engineering from the Federal Institute of Santa Catarina, Florianóplis, Brazil, in 2017, and the M.Sc. degree in electrical engineering from the Federal University of Santa Catarina, Florianóplis, Brazil, in 2019. He is currently working toward the Ph.D. degree with the Centre for Wireless Communications (CWC), University of Oulu, Oulu, Finland.

He is a Researcher with CWC. His research interests include wireless communications, massive machine-type and low-power communications.

Samuel Montejo-Sánchez (Senior Member, IEEE) received the B.Sc., M.Sc., and D.Sc. degrees in telecommunications from the Central University of Las Villas (UCLV), Santa Clara, Cuba, in 2003, 2007, and 2013, respectively.

From 2003 to 2017, he was an Associate Professor with UCLV. Since 2018, he has been with the Programa Institucional de Fomento a la I+D+i, Universidad Tecnológica Metropolitana, Santiago, Chile. He leads the FONDECYT Iniciación No. 11200659 (Toward High-Performance Wireless Connectivity for IoT and Beyond-5G Networks) Project. His research interests include wireless communications, signal processing, sustainable IoT, and wireless RF energy transfer.

Dr. Montejo-Sánchez was a corecipient of the 2016 Research Award from the Cuban Academy of Sciences and was cosupervisor of the awarded Ph.D. Thesis with the 2022 Abertis Award for Research in Road Safety (Ex – Aequo) at the national and international level.

Richard Demo Souza (Senior Member, IEEE) received the D.Sc. degree in electrical engineering from the Federal University of Santa Catarina (UFSC), Florianóplis, Brazil, in 2003.

From 2004 to 2016, he was with the Federal University of Technology—Paraná, Curitiba, Brazil. Since 2017, he has been with UFSC, where he is a Professor with the Department of Electrical and Electronics Engineering. His research interests include wireless communications and signal processing.

Dr. Souza is the Supervisor of the awarded Best Ph.D. Thesis in electrical engineering in Brazil in 2014, and a corecipient of the 2016 Research Award from the Cuban Academy of Sciences. He was an Editor or an Associate Editor for the *SBrT Journal of Communications and Information Systems*, IEEE COMMUNICATIONS LETTERS, IEEE TRANSACTIONS ON VEHICULAR TECHNOLOGY, IEEE TRANSACTIONS ON COMMUNICATIONS, and IEEE INTERNET OF THINGS JOURNAL.

Hirley Alves (Member, IEEE) received the B.Sc. and M.Sc. degrees in electrical engineering from the Federal University of Technology Paraná (UTFPR), Brazil, in 2010 and 2011, respectively, and the dual D.Sc. degree from the University of Oulu, Oulu, Finland, and UTFPR in 2015.

He is the Associate Professor and Head of the Machine-type Wireless Communications Group with the 6G Flagship, Centre for Wireless Communications, University of Oulu, Oulu, Finland. He is actively working on massive connectivity and ultrareliable low-latency communications for future wireless networks, 5 GB and 6G, full-duplex communications, and physical-layer security. He leads the MTC activities for the 6G Flagship Program.

Mr. Alves was a recipient of several awards and has been the Organizer, Chair, TPC, and Tutorial Lecturer for several renowned international conferences. He is the General Chair of the ISWCS'2019 and the General Cochair of the 1st 6G Wireless Summit, Levi 2019, and ISWCS 2021.